

# Dual Mode WECS-Based Two-Stage Hierarchical Control of Hybrid Microgrid



Vipin Kumar Dhiman and Shivam

## 1 Introduction

Due to the high pressure on non-renewable energy sources by nature fundamentalists, the use of renewable energy sources has increased remarkably over the years. Wind energy is one of the widely used renewable energy sources due to its availability. The complete wind energy conversion system (WECS) is one of the fastest-growing energy resources, doubled in the last 10 years. Various WECSs have been proposed by the researchers working under different capacities with different types of generators like double fed induction generator (DFIG), permanent magnet synchronous generator (PMSG) and more [1, 2]. In most cases, WECS comprises a bidirectional converter to link distributed generators (DGs) to AC side main grid and loads. Due to these interconnections, the decreases of system inertia have encountered the problem of maintaining system frequency and voltage for a microgrid. The microgrid can work under grid-connected mode or islanding mode.

In islanding mode, the load demand is met by the WECS DGs with one of the DG should be working as a controlled voltage source [3]. The main concern during this mode is to avoid circulation current while maintaining system frequency and load voltage. During grid-connected mode, the main grid regulates the frequency and voltage because of its large size impact on the system, which removes the extra burden from the microgrid. Also, the bifurcation of active and reactive powers, stable operation and high power quality must be met during the mode of operation.

Depending upon the complications mentioned above, this paper purposed a microgrid two-stage hierarchical control structure for both grid-connected and islanding modes. The primary stage depends upon droop control based on line impedance

---

V. K. Dhiman (✉) · Shivam

Department of Electrical Engineering, NIT Kurukshetra, Kurukshetra, Haryana, India  
e-mail: [vipinkd03@gmail.com](mailto:vipinkd03@gmail.com)

Shivam

e-mail: [shivam55ram@gmail.com](mailto:shivam55ram@gmail.com)

and load characteristics which helps in active and reactive power bifurcation, but its unanimous implementation may lead to deviations in voltage and frequency. So to overcome it, the secondary stage compensates for the deviations in voltage and frequency [4]. Two steps are introduced to enhance the first stage of droop control, with voltage biasing is done using a low bandwidth link in the first step, then voltage magnitude deviations are compensated.

In this paper, a dual-mode WECS is proposed using a two-stage hierarchical control structure. The primary stage performs P-V/Q-f droop control, based upon the active and reactive power-sharing [5]. The secondary stage controls the voltage and frequency fluctuations. The microgrid operates in grid-connected mode with a smooth transition to islanding mode for ensuring synchronization of voltage and frequency within the specified limits. The microgrid included two types of WECS, one is battery-backed to ensure maximum power transfer from wind and storage of surplus power, and the other one is braced by adaptive operation without any storage element.

The performance of the proposed system is investigated under different loading conditions with mode transition. The complete paper is organized as follows: A brief overview of the proposed system and its control is given in Sect. 1. Microgrid and WECS de-tailed topology analysis is discussed in Sect. 2. The proposed dual-stage controller design strategy is covered in Sect. 3. Section 4 presents MATLAB/Simulink environment analysis and validation of the work by different graphs. Finally, in Sect. 5 conclusion is discussed.

## 2 Configuration of Microgrid and Control Structure

### 2.1 WECS-Based Hybrid Microgrid

The microgrid structure is given in Fig. 1 for which the control strategy is proposed which is having two types of wind energy conversion system (WECS) connected to the common microgrid bus. The main AC grid can be connected or disconnected by the means of a static switch. Both types of WECS are having permanent magnet synchronous generator (PMSG) for having higher efficiency, solidity and an acclaimed reputation in offshore wind farms.

### 2.2 WECS-1 Battery Backed

Figure 2 shows the overall formation of the microgrid. The paper does not offer a pitch-plate design of WECS so it's not shown. After the conversion of mechanical to electrical power by WECS-1, it is given to an uncontrolled rectifier via DC-link and boost converter. The maximum power is achieved by the means of wind turbine

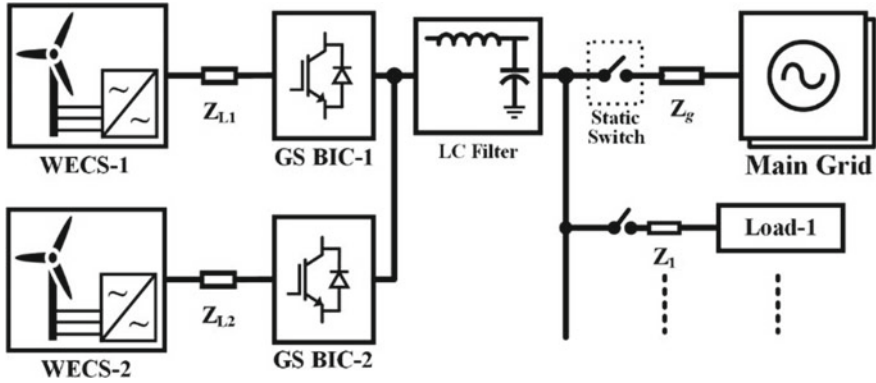


Fig. 1 Configuration of proposed hybrid microgrid

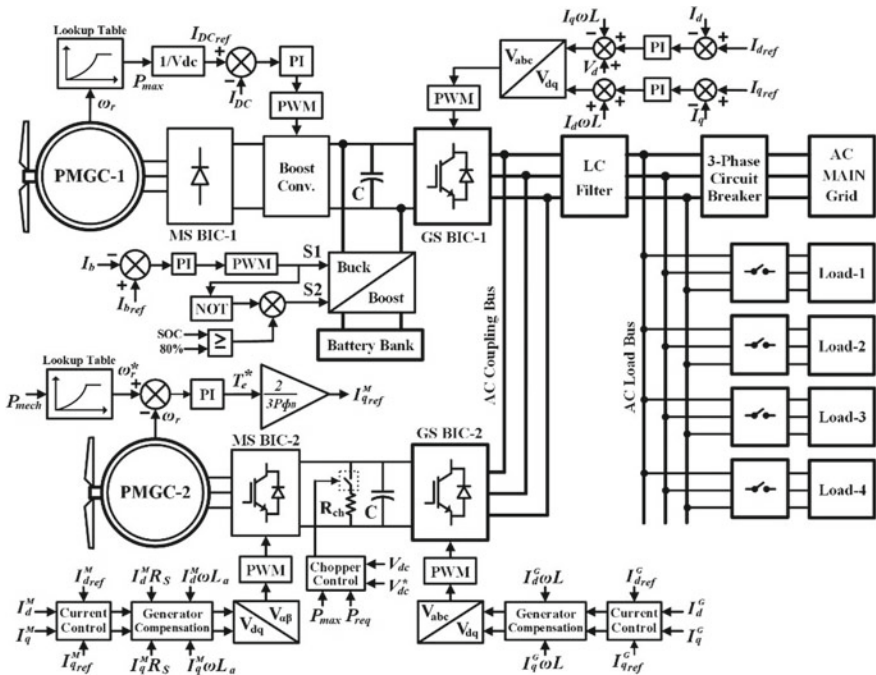


Fig. 2 Structure and control of proposed hybrid microgrid

characteristics and lookup table, further, the buck-boost converter tries to regulate the DC-link voltage by regulating bidirectional battery current. The need for battery becomes unavoidable in islanding mode to regulate DC link voltage and AC side frequency. The battery reference current is defined as:

$$I_{\text{battref}} = k_{bp}(800 - V_b) + k_{bi} \int (800 - V_b)dt \quad (1)$$

where proportional-integral of battery gains are  $k_{bp} - k_{bi}$  with  $V_b$  as battery voltage for the nominal battery of 800 V and 300 kWh.

The main objective of grid side bidirectional converter (GS BIC-1) is to maintain persistent frequency and voltage for microgrid loads, throughout grid-connected mode and islanding mode. For grid-connected mode, active power is given to loads or batteries according to requirement. So two current control loops are adopted for dual-loop control. The primary loop depends upon current references based on coordination control. The secondary loop depends upon the state of charge (SOC) of the battery. Both loops are described in Sect. 3. After converting the current reference in d-q from, a further voltage regulating loop is used. The output voltage after this loop are described after neglecting the effect of filter capacitance:

$$V_{d \text{ out}} = V_d - \omega L i_q + k_{pc_d}(I_{d\text{ref}} - I_d) + k_{ic_d} \int (I_{d\text{ref}} - I_d)dt \quad (2)$$

$$V_{q \text{ out}} = \omega L i_d + k_{pc_q}(I_{q\text{ref}} - I_q) + k_{ic_q} \int (I_{q\text{ref}} - I_q)dt \quad (3)$$

where  $\omega L$  is the settlement portion for filter inductance,  $k_{pc_d}$ ,  $k_{ic_d}$ ,  $k_{pc_q}$  and  $k_{ic_q}$  are P-I gains of d-q current regulators respectively [6].

### 2.3 WECS-2: Adaptive Operated

As shown by Fig. 2, the second type WECS utilizes controlled converters at both grid-side and machine-side. The machine-side BIC is used to extract max power by wind turbine. It uses MPPT algorithm by analyzing rotor speed  $\omega_r$  to achieve maximum active current  $I_q$ . The reference current for this converter in dq-frame are:

$$I_{d \text{ ref}}^M = 0 \quad (4)$$

$$I_{q \text{ ref}}^M = \frac{2T_e^*}{3P\phi_B} \quad (5)$$

$$T_e^* = K_{p_t}(\omega_r^* - \omega_r) + K_{i_t} \int (\omega_r^* - \omega_r)dt \quad (6)$$

where  $T_e^*$  is pre-set electrical torque, is  $P$  pole pairs,  $\phi_B$  is generator magnetic flux,  $\omega_r^*$  is reference rotor speed,  $K_{p_t}$  and  $K_{i_t}$  are the P-I gains for torque regulator.

To avoid power imbalance in islanding mode, WECS-2 utilises the adaptive operation as in this mode real power required could be less than the generated power, which is done by proper active-reactive current references. The active-reactive current

reference is set as:

$$I_{d\text{ref}}^G = \min \left\{ K p_{DC}L (V_{DC}^* - V_{DC}) + K i_{DC}L \int (V_{DC}^* - V_{DC}) dt \right. \quad (7)$$

$$\left. \frac{2P_{\text{req}}}{3V_d} \right\}$$

$$I_{q\text{ref}}^G = K p_r (Q_{\text{req}} - Q_{\text{avl}}) + K i \int_r^d (Q_{\text{req}} - Q_{\text{avl}}) dt \quad (8)$$

$$Q_{\text{avl}} = \frac{3}{2} V_d^I I_{q\text{avl}} \quad (9)$$

where  $V_d$  is d-axis voltage,  $P_{\text{req}}$  is real power needed by the microgrid,  $I_{q\text{avl}}$  is available reactive current,  $Q_{\text{req}}$  and  $Q_{\text{avl}}$  are the required and available reactive power, and  $K_{p_r} - K_{i_r}$  are the proportional-integral gains. It is to be noted that  $Q_{\text{req}}$  must be restricted to  $Q_{\text{avl}}$  as a threshold boundary.

To achieve optimum DC link voltage, the modulation signal for chopper  $m_{ch}$  and maximum chopper power  $P_{ch}$  is given as:

$$m_{ch} = \frac{K p_{ch} (V_{DC}^*{}^2 - V_{DC}^2) + K i_{ch} \int (V_{DC}^*{}^2 - V_{DC}^2) dt + \sqrt{(P_{\text{max}} - P_{\text{req}})^2 - Q_{\text{req}}^2}}{P_{ch}} \quad (10)$$

$$P_{ch} = \frac{V_{DC}^2}{R_{ch}} \quad (11)$$

where  $K_{p_{ch}}$  and  $K_{i_{ch}}$  are P-I gain of chopper regulator [7].

### 3 Proposed Two-Stage Hierarchical Control System

#### 3.1 Primary Stage

To achieve the synchronous generator-like behaviour, P-V/Q-f droop control is utilised as the primary control stage. At this stage, real power adjustment is linked with frequency and reactive power is with the profile of voltage. The consideration of a small system with low voltage microgrids is to be taken for having the line impedance rate ( $R/X_L$ ) significantly large. So, the line-impedance characteristics consider as mostly resistive with real and reactive powers are calculated as:

$$P = \frac{V \cdot E - V^2}{Z} \quad (12)$$

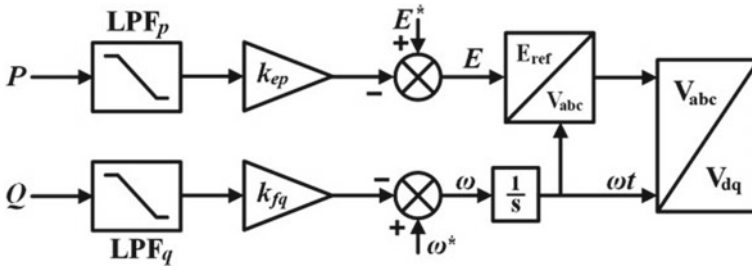


Fig. 3 Primary stage droop control

$$Q = -\frac{V \cdot E}{Z} \varphi \quad (13)$$

where  $V$  is grid voltage,  $E$  is output voltage of inverter  $Z$  and  $\varphi$  are line impedance with its phase angle. The real power depends upon variation in voltage while reactive power is on phase angle. So, the droop equations for resistive lines expressed as:

$$E^* - E = k_{ep} P_{\text{mesr}} \quad (14)$$

$$\omega^* - \omega = k_{fq} Q_{\text{mesr}} \quad (15)$$

where  $\omega^*$  and  $E^*$  are predefined angular frequency and voltage,  $k_{ep}$  and  $k_{fq}$  are active-reactive droop coefficients power, and defined by Eqs. (16) and (17),  $P_{\text{mesr}}$  and  $Q_{\text{mesr}}$  are measured real and reactive power resulting by Eqs. (18) and (19) [6] (Fig. 3).

$$k_{ep} = \frac{V_h - V_l}{P_h} \quad (16)$$

$$k_{fq} = \frac{\omega_h - \omega_l}{Q_h} \quad (17)$$

$$P_{\text{mesr}} = \frac{\omega_c}{\omega_c + s} P \quad (18)$$

$$Q_{\text{mesr}} = \frac{\omega_c}{\omega_c + s} Q \quad (19)$$

where  $\omega_h$ ,  $\omega_l$ ,  $V_h$  and  $V_l$  are the highest and lowest permissible sets of frequency and voltage.  $P_h$  and  $Q_h$  are the highest permissible real and reactive power with the cut-off frequency of low pass filter is  $\omega_c$ .

The expression of pre-set current for grid side converter with power transfer can be given as:

$$I_{\text{pre}} = 2P_{\text{Trans}}/3V_{od} \quad (21)$$

$$P_{Trans} = \frac{3}{2}V_{od}I_{od} + \frac{3}{2}V_{oq}I_{oq} \tag{22}$$

where d-q frame reference output voltages and current are  $V_{od}, V_{oq}, I_{od}$  and  $I_{oq}$  for grid side converter [8].

### 3.2 Secondary Stage

During load fluctuation and non-uniform generation, the change in voltage and frequency should be bound in the specified limits. At this stage, to die out these undesirable changes, voltage and frequency are compared with pre-set values. The differences found are injected back or removed using PI controllers to the initial stage. The compensation is done with load voltage in d-q reference frame with a comparison of primary stage droop control. The resultant d-q axis newly established of voltages are given as:

$$V_d^{**} = V_d^* + K_{p_{d\ sec}}(V_d^* - V_{dL}) + K_{i_{d\ sec}} \int (V_d^* - V_{dL})dt \tag{22}$$

$$V_q^{**} = V_q^* + K_{p_{q\ sec}}(V_q^* - V_{qL}) + K_{i_{q\ sec}} \int (V_q^* - V_{qL})dt \tag{23}$$

where  $K_{p_{d\ sec}}$  and  $K_{i_{d\ sec}}$  are d-axis secondary P-I gains,  $K_{p_{q\ sec}}$  and  $K_{i_{q\ sec}}$  are q-axis secondary PI gains,  $V_{dL}$  and  $V_{qL}$  are real-time d-q reference frame load voltages (Fig. 4).

For the advancement of the secondary stage, two active and reactive terms ( $\delta P$  and  $\delta Q$ ) for load damping are added to the above equations [9]. The purpose is to safeguard the integral control loop which was becoming more influenced due to continuous load variations. After taking  $\alpha$  as active load-damping and  $\beta$  as the reactive load-damping, the advanced d-q reference frame voltages are established as:

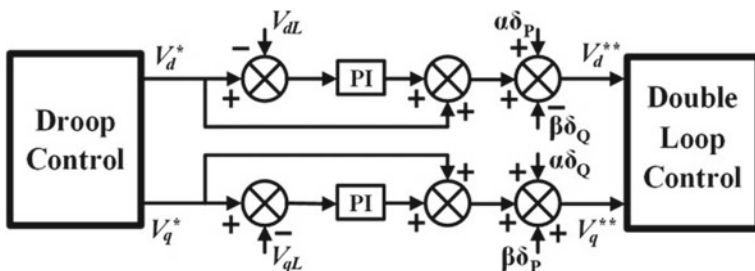


Fig. 4 Proposed secondary-stage droop control

$$V_d^{**} = V_d^* + K_{pdsec}(V_d^* - V_{dL}) + K_{idsec} \int (V_d^* - V_{dL})dt + \alpha\delta_P - \beta\delta_Q \quad (24)$$

$$V_q^{**} = V_q^* + K_{pqsec}(V_q^* - V_{qL}) + K_{idsec} \int (V_q^* - V_{qL})dt + \beta\delta_P + \alpha\delta_Q \quad (25)$$

$$\delta_P = \frac{dP_{Load}}{dt}, \text{ if } \frac{dP_{Load}}{dt} > \frac{dP_{WD}}{dt}; \text{ or else } 0 \quad (26)$$

$$\delta_Q = \frac{dQ_{Load}}{dt}, \text{ if } \frac{dQ_{Load}}{dt} > \frac{dQ_{WD}}{dt}; \text{ or else } 0 \quad (27)$$

where  $P_{Load}$  and  $Q_{Load}$  are load real and reactive powers,  $P_{WD}$  and  $Q_{WD}$  are real and reactive powers of WECS. It is to be noted that values of  $\delta_P$  and  $\delta_Q$  are taken as zero when power output from wind is lessor than load power.

### 4 Results and Analysis

In this section, MATLAB/Simulink-based model on the proposed dual-stage hierarchical control of hybrid microgrid with two types of WECS is constructed, simulated and analysed. Based on the related theory formation in the above sections, two modes are considered as grid-connected mode and islanding mode with their transition. Table 1 describes the transition period while Table 2 describes the system parameters. During the whole operation and transition, both WECS, battery-bank and AC loads are uninterruptedly associated while the AC main grid is detached from the system at 2 s by three-phase circuit breaker as static switch henceforth the system drives to islanding mode.

#### 4.1 Grid-Connected Mode

For an initial 0–2 s, the AC main grid is linked to the system henceforth system remained in grid-connected mode, while an AC load 2 of 50 + j20 kVA is added at 1 s to verify the loading effect on the system. For the WECS-1, the DC link voltage

**Table 1** Operational periods

Case	Operation mode	Time (s)	Modification
A.	Grid-connected mode (up to initial 2 s)	1	Load-2 added
		2	Gird disconnection
B.	Islanding mode (after initial 2 s)	3	Load-2 removed
		3.5	Load-3 removed



**Table 2** System parameters

Sl. No.	Parameter names	Ratings
1.	WECS-1	360 kVA
2.	WECS-2	300 kVA
3.	Battery capacity of WECS-1	300 kWh
4.	DC link capacitance in WECS-2	3.5 mF
5.	AC main grid voltage	480 V
6.	System frequency	50 Hz
7.	Feeder Impedance	$0.1 + j0.018 \Omega$
8.	Loads: 1, 2, 3 and 4 respectively	100, 50 + j50, 50, 50 + j20 kVA

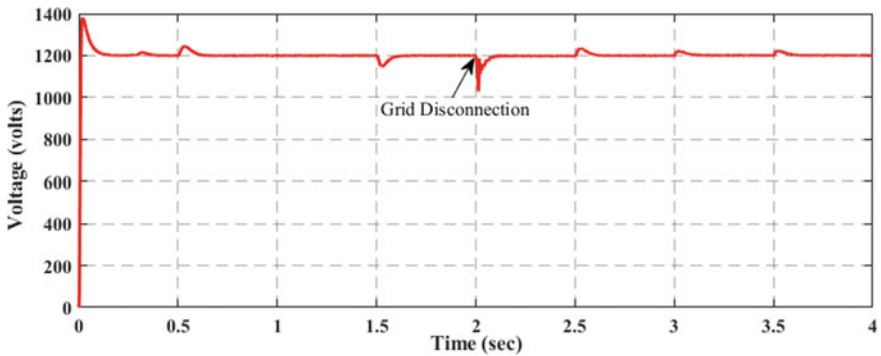


**Fig. 5** DC-link voltage at WECS-1

is maintained at the level of 1200 V as shown by Fig. 5. Initially, after the transient period over the first stage of droop control and charge controller of battery helps to maintain the DC- link voltage at the desired level with minimal variations [10]. The AC load-side frequency is shown by Fig. 6, it has a small variation during mode transition at 2 s and load addition at 3 s. The battery SOC is shown in Fig. 7, the battery is charging by storing extra power available. Figure 8 shows the AC side voltage and current at the main grid and loads, at 2 s when AC main grid is separated from the system, then the grid voltage and the current becomes zero p.u. as required and for loads, the voltage remains almost 1 p.u. while load current is changing according to the requirements, supported by taking power from both WECS. Figure 9 shows the active and reactive powers provided by the AC main grid and consumed by AC loads. During this mode, real and reactive power for the loads is mainly provided by the AC main grid and becomes zero after this mode at 2 s. Figure 9 shows the active and reactive power provided by both WECS, for WECS-1 during grid-connected mode real power is provided to the battery while WECS-2 provides power to load throughout the operation because its system does not have energy storage devices.

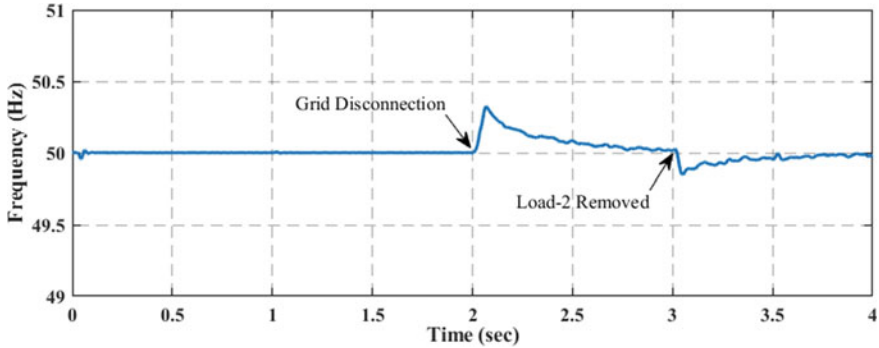


Fig. 6 Load frequency of the system

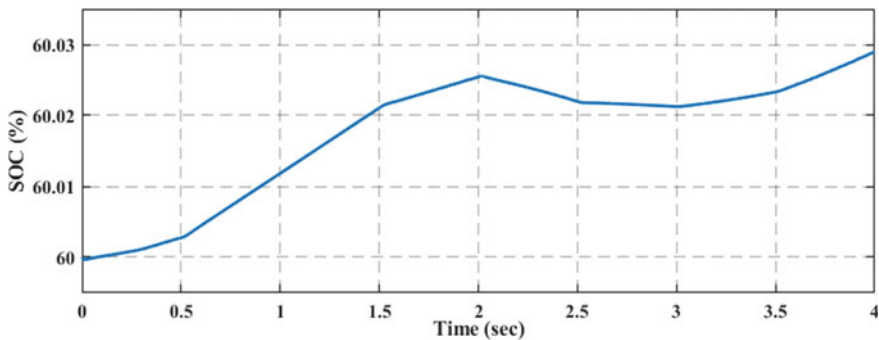


Fig. 7 Battery SOC

During this mode, the reactive power is mainly provided by the AC main grid for maintaining proper operation.

For considering the change effect of loads on the system, load 2 is added to the system at 1 s, the real and reactive power requirement increases as shown in Fig. 9. At this change magnitude of current at the grid and load is increased because of load change while voltages are maintained at the same level. At this instant other DC bus voltage, system frequency and SOC of the battery remain the same.

## 4.2 Islanding Mode

The mode transition from grid-connected mode to islanding is performed at 2 s by removing the AC main grid from the system using a 3-phase circuit breaker as a static switch. At this instant, system performance is critically decisive as the system can go into an unstable mode. At this instant, all the loads are connected to the system which

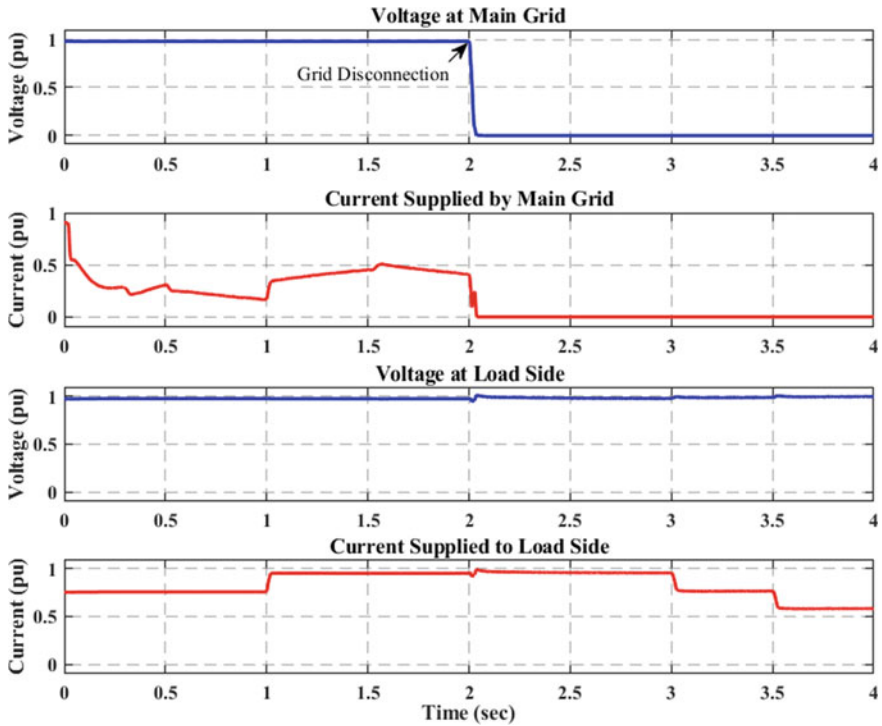


Fig. 8 Voltages and currents at the main grid and load

gets power from the two WECS. The proposed control strategy helps to achieve the above mode transition reliably.

At the starting of this islanding mode, the DC bus voltage for WECS-2 has a dip but recovers instantly to 1200 V as shown by Fig. 5, further have small variations which are in limits [6]. Figure 6 indicates the system frequency which increases a bit from its desired value of 50 Hz, droop control further maintains system frequency within operational limits. The battery SOC indicates discharging but after a small instant it again starts charging by taking surplus power from WECS-2 as shown by Fig. 7. The voltage and current at the main grid become zero and a small variation is observed in the load voltage which decays out further as shown by Fig. 8 and the load current is maintained according to the load demand supported by grabbing power from both WECS. The real and reactive powers provided by the AC main grid becomes zero throughout this mode shown by Fig. 9. The required real and reactive powers for loads are supplied from both WECS as mentioned above and shown by Fig. 10.

Further to observe load variations, at 3 s load-2 and at 3.5 s load-3 is removed from the system, the current supplied to load indicates a dip in its value as shown by Fig. 8. At the same time power supplied from WECS increased because power requirement decreased at load. A small dip in the system frequency is observed at

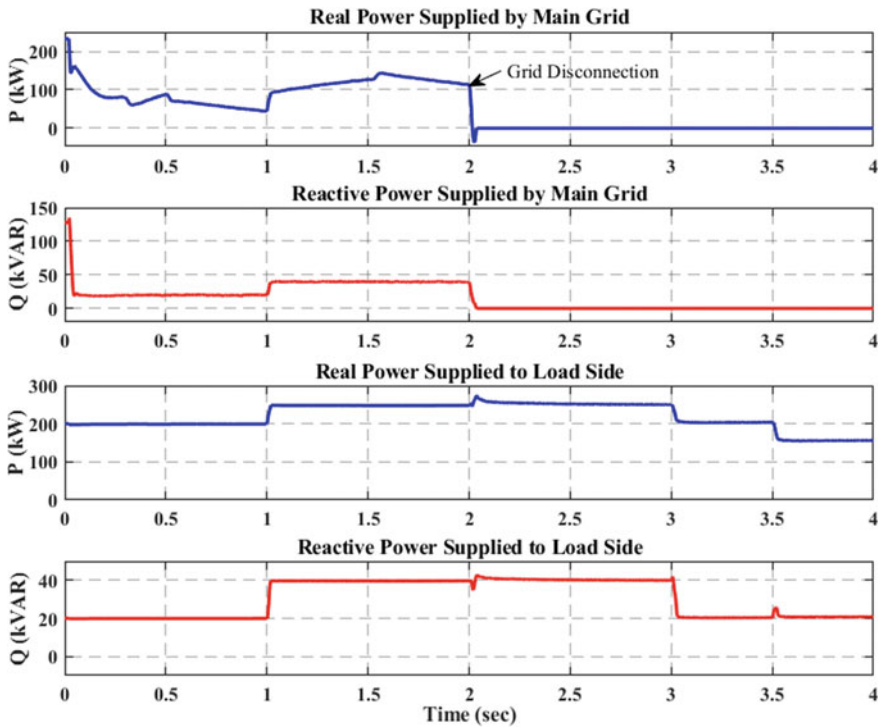


Fig. 9 Real and reactive powers at the main grid and load

3 s due to the load removed which is further maintained at the desired level. During mode transition and load variation throughout the whole simulation, load voltage remains almost constant (Table 3).

## 5 Conclusion

The modelling, examination and simulation of the dual-stage hierarchical control strategy for coordinating two types of WECS with AC main grid are seamlessly performed in the MATLAB/Simulink environment. The battery-backed WECS-1 extracts maximum power from the wind during both grid-connected and islanding mode of operation. The battery-free WECS-2 supported by adaptive control helps to avoid power imbalance and improves system flexibility. The structure of two-stage hierarchical control consists PV/Q-f droop control as the primary stage whose task to share real and reactive power was found satisfactory. The secondary stage improves transients stability by compensating the deviations in load voltage and current, further to support overshoot damping during large load change two damping terms were added in each d-q frame. Moreover, the dual-stage control strategy also

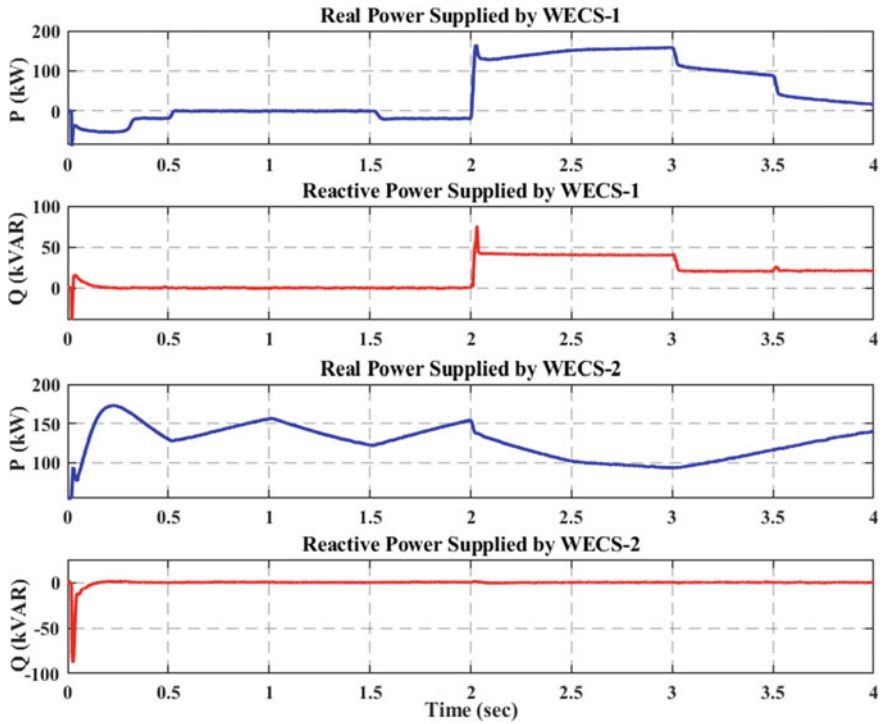


Fig. 10 Real and reactive power supplied by two WECS

Table 3 Control parameters

Sl. No.	Parameter names	Ratings
1.	WECS-1 grid side converter voltage regulator PI gains for d-q axis respectively	0.86, 4.89; 0.65, 4.6
2.	WECS-1 grid side converter current regulator PI gains for d-q axis respectively	3.3, 40; 1.8, 66
3.	WECS-1 current regulator PI gains for DC boost converter	0.56, 13.8
4.	WECS-1 current regulator PI gains for DC buck boost converter	4.5, 60
5.	WECS-2 grid side converter current regulator PI gains for d-q axis respectively	5.4, 82; 10.6, 63
6.	WECS-2 grid side DC regulator PI gains	18, 78
7.	WECS-2 chopper voltage controller PI gains	0.2, 6.9

(continued)

**Table 3** (continued)

Sl. No.	Parameter names	Ratings
8.	WECS-2 machine side converter current regulator PI gains for d-q axis respectively	4, 12; 4, 14
9.	Current compensator PI gains for unplanned outage	5, 52
10.	Pre-synchronized controller PI gains for voltage, frequency and phase angle respectively	0.2, 4; 4.2, 2; 12, 7.5
11.	Active load damping adaptive gain, $\alpha$	0.65
12.	Reactive load damping adaptive gain, $\beta$	0.25

regulates DC bus voltage for WECS-1, system frequency and power bifurcation and transition of grid-connected mode to islanding mode even though load variations.

## References

1. K.B. Tawfiq, A.S. Mansour, H.S. Ramadan, M. Becherif, E.E. El-Kholy, Wind energy conversion system topologies and converters: comparative review. *Energy Proc.* **162**, 38–47 (2019)
2. S. Muhammad, S. Imran, R. Shafiqur, K. Shamim, M.A. Luai, Assessment of wind energy potential using wind energy conversion system. *J. Clean. Prod.* **216**, 346–360 (2019)
3. X. Tang, X. Hu, N. Li, W. Deng, G. Zhang, A novel frequency and voltage control method for islanded microgrid based on multienergy storages. *IEEE Trans. Smart Grid* **7**, 410–419 (2016)
4. L. Che, M. Shahidehpour, A. Alabdulwahab, Y. Al-Turki, Hierarchical coordination of a community microgrid with AC and DC microgrids. *IEEE Trans. Smart Grid* **6**(6), 3042–3051 (2015)
5. M. Rezkallah, A. Chandra, B. Singh, S. Singh, Microgrid: configurations, control and applications. *IEEE Trans. Smart Grid* **10**(2), 1290–1302 (2019)
6. V.K. Dhiman, Shivam, Enhanced two-stage coordination control of AC/DC hybrid microgrid, in *2020 IEEE 9th Power India International Conference (PIICON)*, SONEPAT, India, 2020, pp. 1–6
7. U.K. Kalla, H. Kaushik, B. Singh, S. Kumar, Adaptive control of voltage source converter based scheme for power quality improved grid-interactive solar PV–battery system. *IEEE Trans. Ind. Appl.* **56**(1), 787–799 (2020). <https://doi.org/10.1109/tia.2019.2947397>
8. P. Omid, K. Kimmo, Hierarchical control structure in microgrids with distributed generation: Island and grid-connected mode. *Renew. Sustain. Energy Rev.* **44**, 797–813 (2015)
9. J.M. Guerrero, J.C. Vasquez, J. Matas, L.G. de Vicuna, M. Castilla, Hierarchical control of droop-controlled AC and DC microgrids—a general approach toward stand-ardization. *IEEE Trans. Industr. Electron.* **58**(1), 158–172 (2011)
10. IEEE Standard for the Specification of Microgrid Controllers,” in *IEEE Std 2030.7–2017*, (2018), pp. 1–43. Accessed 23 April 2018